Writhe and mutual entanglement combine to give the entanglement length

E. Panagiotou,[1,*] M. Kröger,[2,†] and K.C. Millett[1]

[1] *Department of Mathematics, University of California, Santa Barbara, California 93106, USA*
[2] *Polymer Physics, Department of Materials, Wolfgang-Pauli-Str. 10, CH–8093 Zurich, Switzerlamd*

We propose a new method to estimate N_e, the entanglement length, that incorporates both local and global topological characteristics of chains in a melt under equilibrium conditions. This estimate uses the writhe of the chains, the writhe of the primitive paths and the number of kinks in the chains in a melt. An advantage of this new method is that it works for both linear and ring chains, works under all periodic boundary conditions, does not require knowing the contour length of the primitive paths and it does not rely on a smooth set of data. We apply this method to linear finitely extendable non-linear elastic chains and we observe that our estimates are consistent with those from other studies.

PACS numbers: 83.80.Sg, 02.10.Kn, 83.10.Kn, 05.40.Fb
Keywords: FENE chains, topology, writhe, entanglements, wormlike chains, knots

I. INTRODUCTION

The rheological properties of polymer melts are determined primarily by the random-walk-like structure of the constituent chains and the fact that the chains cannot cross. The motion of sufficiently long chains is limited by the presence of the other chains which create persistent obstacles, called *entanglements*. As the degree of polymerization becomes larger than the *entanglement length*, N_e, the entanglements become important and dramatically change many melt properties such as diffusivity and viscosity. In entangled polymer melts and solutions, N_e is arguably the most fundamental material parameter which can be measured experimentally by the *plateau modulus*.

Edwards suggested that entanglements effectively restrict individual chain conformations to a curvilinear tubelike region enclosing each chain [1]. For very short time scales, chain segments are allowed to freely fluctuate in all directions until their displacements become commensurate with the tube diameter, a, which is related to entanglement length by $a^2 = N_e b$, where b is the bond length [2–4]. Thus, N_e characterizes the crossover between the Rouse and the reptation regime and it is commonly interpreted as the number of monomers between entanglements. The axis of the tube is a coarse-grained representation of the chain, called the *primitive path* (PP). Edwards defined the PP as the shortest path a chain, fixed at its ends, can follow without crossing any other chains. Based on this definition, Rubinstein and Helfand [5] realized that the entanglements in a system could be obtained by reducing all chains to their PPs simultaneously, creating a PP network. Since then several methods have been developed for extracting the PP network [6–10]. Two geometrical methods capable of efficiently reducing computer generated polymer models to entanglement networks are the Z1-code [7, 8, 11] and the CReTA algorithm [9]. All the methods work in discontinuous coordinate space; ie., they use finite displacements during which disentanglement events must be avoided. Despite differences in their specific implementation, these methods are reported to yield similar results for the average properties of the PP network [8]. These algorithms extract the PP network estimate of N_e either from the chain statistics of the PPs or from direct enumeration of entanglements, defined as contacts between PPs. The different approaches produce somewhat different results for N_e for the same atomistic configurations [4, 8, 9, 12, 13]. Indeed, the resulting PP network is not unique and several of its features such as the role of self-entanglement, the difference between energy minimization and length minimization, the location of entanglement points along a PP, have been examined [7–9, 14–18]. Notice that the process of drawing the strands tight destroys the detailed geometry of the melt and these methods may lead one to think of entanglements as local binary contacts between two chains. To better capture the geometry, other methods to extract the PP, such as the time isoconfigurational average [19–21], have been proposed.

Despite these advances, our understanding of entanglement is incomplete. The reason is the difficulty to connect the entanglement properties of the chains at two different scales. In the rest of this paper we shall call the local obstacles to the motion of the chains, *local entanglement*, and we shall call the conformational complexity of the entire conformations of the chains in the melt, *global entanglement* (see Fig. 2 for an illustrative example). Edwards first pointed out that in the case of ring polymers, the global entanglement of the chains can be studied by using tools from mathematical topology, such as the Gauss linking number [22, 23]. First, notice that the uncrossability of the chains allows them to attain only *isotopic* configurations, that is, configurations that are related by continuous deformations that do not allow intersections. This notion of isotopy is a basic concept in topology. Under certain conditions, we can model the polymer chains as simple mathematical curves in space. A *knot* (resp. *link*) is one (or more resp.) simple closed curve(s) in space without intersections. The complexity (or topological state) of these knots or links is related to their global entanglement and it can be measured by using *topological invariants* such as knot or link polynomials [24–27]. The topological invariants are properties of knots or links, which are the same for isotopic configurations. Since Edwards, many studies have been devoted to the topology of

* Corresponding author: panagiotou@math.ucsb.edu
† Website: http://www.complexfluids.ethz.ch

polymer rings and its relation to physical properties [6, 28–31]. The study of global entanglement has been very useful especially in the study of biopolymers [32, 33]. In [30] a direct relation between distinct topological states and N_e has been revealed. Therein, N_e was estimated for a system of ring polymers in one or two PBC, using purely topological tools, ie. the Jones and the HOMFLY polynomials [24, 26, 30]. One of the reasons why this has not been explored as much in the case of polymer melts is because of the problem of dealing with linear polymers. In the case of linear polymers, the notion of topological invariant does not apply since topological open curves can be continuously deformed to attain any configuration. Efforts have been made to characterize the knotting of an open chain [29, 34–36]. For example one can use the methods described in [35, 36] to determine the spectrum of knotting arising from the distribution of knot types created by closure of the open chain to the "sphere at infinity". In this study we will measure the global entanglement of open chains directly without employing any closure. Our goal is to provide a method to estimate N_e for a melt of both linear or ring polymers in any PBC model by combining the local and global entanglement characteristics of the chains in a melt.

A measure of global entanglement, that is meaningful both for closed or open chains, is the *Gauss linking integral*. For two closed chains (ring polymers) the Gauss linking integral is a topological invariant that measures the algebraic number of times one chain turns around the other. For two open chains (linear polymers), it is a real number that is a continuous function of the chain coordinates. The Gauss linking integral can be also applied to one chain in order to provide a measure of global self-entanglement of a chain, called the *writhe* [37–42]. The writhe is a real number that changes continuously under continuous deformations of a chain. The writhe is very clearly not a topological invariant, even for closed chains, because it is a quantity that depends on the specific geometry of the chain, and it is very sensitive to the specific conformations that are analyzed. Computer experiments indicate that the linking number and the writhe are effective indirect measures of global entanglement in systems of random filaments [22, 28, 31, 43–51]. Analytical and numerical results have shown that the writhe of random walks and polygons depends on their length and that it follows a different scaling for random walks in a lattice, or under confinement [38, 49, 52–63]. Kholodenko and Vilgis [64] have proved that the writhe of semi-flexible rings follows a scaling that depends both on the stiffness parameter and on the length of the chains.

The information provided by the writhe is very useful but it is not clear how to put it into the context of current tube and slip-link model methods [65]. In this paper we show that the writhe in combination with the Z1 algorithm can provide new information that is relevant to the physical notions of entanglement, such as N_e-estimators, denoted $\mathcal{N}_e(N)$, that aim at estimating $N_e = \lim_{N\to\infty} \mathcal{N}_e(N)$ from information derived from a finite number of monomers per chain, N. The paper is organized as follows: In Section II we describe the measures of entanglement that are used in this paper. In Section II B 1 we numerically study the mean absolute writhe of semi-flexible linear chains in order to extend the analytical result of Kholodenko and Vilgis [64] to open chains. We will use this in the following section in order to estimate N_e for linear chains in a melt. In Section III a new N_e-estimator is introduced based on the writhe of the original chains, the writhe of their PPs and the number of kinks. In Section IV we compute the new N_e-estimator for linear, finitely extendible nonlinear elastic FENE chains in a melt and compare it with the results of previous estimators for the same system. Next, in Section V, we discuss some results stemming from the earlier analysis concerning the number of kinks, the writhe of the original chains, the writhe of their PPs and the writhe of the entanglement strands. These provide further insight to the global and local entanglement of the system.

II. MEASURES OF ENTANGLEMENT OF A LINEAR POLYMER CHAIN IN A MELT

To measure the entanglement of polymer chains in a melt we measure their writhe and use the Z1 algorithm to determine their PP. This section is devoted to their description.

A. Z1 algorithm

The Z1 algorithm [11] is a state-of-the-art geometric algorithm which proceeds by transforming the physical picture of topological interchain constraints (as conceived by Doi- Edwards [1]) into a pure mathematical problem of identifying the shortest multiple disconnected (primitive) path subject to geometrical constraints arising from the configuration of the corresponding atomistic system. More precisely, given a fixed polymer melt configuration, the algorithm minimizes the contour length of the chains by moving the beads sequentially in space maintaining the noncrossability of the chains. In this way the chains become rectilinear strands coming together at kinks where the entanglements occur. Disentanglement is prevented by constraining moves of kinks to lie in the plane of their adjacent segments. The Z1 code provides the option to respect or neglect self-entanglements, that is, kinks between arcs of the same chain. Computational effort is, in both cases, very comparable. For a system of M chains of N monomers each, the computational effort of the Z1 algorithm is of the order $M\,N$, ie. almost linear in the total number of monomers [7]. In previous studies it has been shown that self-entanglements between distant chain sections in polymer melts are rare [14]. In this study, to allow for a direct comparison with previous works [13], we use the version of Z1 that does not capture self-entanglements. We stress that, even if there are no kinks of a chain with itself, this does not mean that a chain is not entangled with itself at a global level. This global self-entanglement is imposed to a chain due to the presence of the other chains (see Fig. 2 for an illustrative example). Thus, even if self-crossings are allowed, on average the global self-entanglement remains due to the uncrossability with other chains.

A direct consequence of the specific mathematical formulation is that the Z1 algorithm provides as output the average

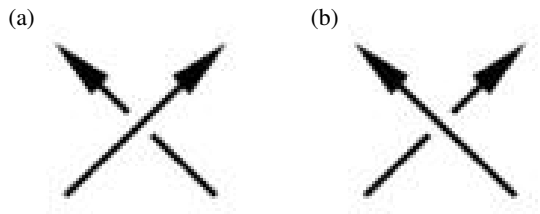

FIG. 1. (a) $+1$ crossing and (b) -1 crossing. By assigning a sign to each crossing, one recovers information concerning which arc comes over and under.

contour length of a primitive path, $\langle L_{\rm pp}\rangle$. Here and in the following, $\langle\ \rangle$ denotes averaging over all chains of a given configuration. In addition, by mapping the extracted interior nodes of each primitive path into kinks, the average number of interior kinks (entanglements), $\langle Z\rangle$, per chain is returned. The probability distribution of $\langle Z\rangle$ has been approximated by a Poissonean [15, 66] (Appendix D). We will use the following notation for the average values of these quantities over all chains: $\mathcal{Z} = \langle Z\rangle$ and $\mathcal{L}_{\rm pp} = \langle L_{\rm pp}\rangle$. Finally, from the output of Z1 one can recover N_e values in accordance with experiments [13] (Section IV A).

B. The writhe of a curve

Consider a frozen configuration of polymer chains represented by a collection of polygonal curves in three-dimensional space. A simple measure of global self-entanglement for individual chains is given by counting the crossings in a random projection of one or two chains. Indeed, notice that in all generic orthogonal projections of a planar curve one would not see any crossings. Similarly, for two unlinked planar curves, almost all projections would give no crossings between them. Without loss of generality, we can assign an orientation to the chains. By assigning a sign to each crossing (Fig. 1), one can recover information concerning which arc passes over and under the other. To appreciate the character of the *writhe* of a chain we first introduce a *linking number*. We follow the presentation in [62].

For a generic projection of two oriented curves l_1, l_2 to a plane defined by a vector $\boldsymbol{\xi} \in S^2$ the *linking number of a diagram*, denoted $lk_{\boldsymbol{\xi}}(l_1, l_2)$, is equal to one half the algebraic sum of crossings between the projected curves. The *linking number* of two oriented curves is then equal to the average linking number of a diagram over all possible projection directions, ie. $L(l_1, l_2) = (4\pi)^{-1}\int_{\boldsymbol{\xi}\in S^2} lk_{\boldsymbol{\xi}}(l_1, l_2)\mathrm{d}S$. This can also be expressed by the Gauss linking integral for two oriented curves. The Gauss *linking number* of two oriented curves l_1 and l_2, whose arc-length parametrization is $\gamma_1(t), \gamma_2(s)$ respectively, is defined as a double integral over l_1 and l_2 [67]:

$$L(l_1, l_2) = \frac{1}{4\pi}\int\limits_{[0,1]}\int\limits_{[0,1]} \frac{(\dot\gamma_1(t), \dot\gamma_2(s), \gamma_1(t) - \gamma_2(s))}{|\gamma_1(t) - \gamma_2(s)|^3}\,\mathrm{d}t\mathrm{d}s \tag{1}$$

where the nominator of the integrand is the triple product of $\dot\gamma_1(t), \dot\gamma_2(s)$ and $\gamma_1(t) - \gamma_2(s)$.

Similarly, for the generic orthogonal projection of one oriented curve l to a plane defined by a vector $\boldsymbol{\xi} \in S^2$ we define the *writhe of a diagram*, denoted $Wr_{\boldsymbol{\xi}}(l)$ to be equal to the algebraic sum of crossings of the projection of the curve with itself. Then the *writhe* of a curve is defined as the average writhe of a diagram of the curve over all possible projections, ie. $Wr(l) = (4\pi)^{-1}\int_{\boldsymbol{\xi}\in S^2} Wr_{\boldsymbol{\xi}}(l)\mathrm{d}S$. Analogously, this can be expressed as the Gauss linking integral over one curve. The *writhe* of an oriented curve l with arc-length parametrization $\gamma(t)$ is thus alternatively and more conveniently defined by the Gauss linking integral over a curve

$$Wr(l) = \frac{1}{2\pi}\int\limits_{[0,1]^*}\int\limits_{[0,1]^*} \frac{(\dot\gamma(t), \dot\gamma(s), \gamma(t) - \gamma(s))}{|\gamma(t) - \gamma(s)|^3}\,\mathrm{d}t\mathrm{d}s \tag{2}$$

where $[0,1]^* \times [0,1]^* = \{(x,y) \in [0,1]\times[0,1] | x \neq y\}$.

We observe that the geometrical meaning of the writhe and the linking number is the same for open or closed curves, it is the average over all projection directions of the algebraic sum of crossings, or inter-crossings respectively, in the projection of the curve, or curves respectively. When applied to open chains both measures are continuous functions in the space of configurations. Furthermore, as the endpoints of the curves move towards coincidence, the linking number or writhe tend to the values of those measures for the resulting closed knots or links. In the case of closed chains the linking number is a topological invariant.

For a polygonal curve the Gauss linking integral can be easily computed following the algorithm described in [39]. More precisely, for a system of M chains of N monomers each, the computation of the writhe for all chains is of the order $M\,N(N-1)/2$. It has been shown numerically that the writhe follows a normal distribution [61], centered around zero. For a system of many chains in a simulation box, and a large sample, the statistics of the writhe could be estimated from a subset of the chains in each polymer melt configuration. If only a fraction $\sim 1/N$ of all chains (requiring $M \gg N$) is sufficient to estimate the writhe, the computational effort is of the order of the Z1 code, $M\,N$.

In the following we will take averages of the writhe of polymer chains in melts simulated with the use of a periodic box. The periodic box is replicated in space to form a large bulk system. As it has been pointed out in previous studies [30, 68, 69], the periodicity of the chains induces special features in the global entanglement of the melt. For a system with M chains in a periodic box, there are only M different conformations in the periodic system that the box generates and infinitely many copies of these conformations. In this study we will use the writhe to measure the global self-entanglement characteristics per chain in the periodic system. Thus, for a

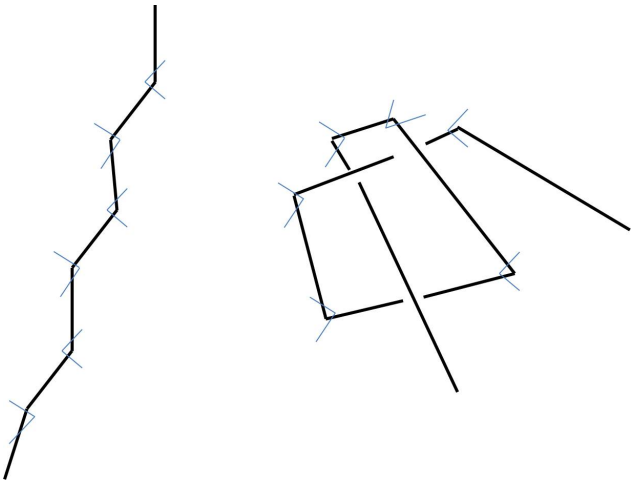

FIG. 2. Example of two conformations with the same number of kinks, $Z = 6$, but with different writhe, $Wr = 0.007$ and $Wr = 2.78$, respectively. We notice that the conformation of the first chain is simple, while the other is more complex. A direct end-to-end closure of the first chain will produce the unknot (the trivial knot type), while the direct end-to-end closure of the second results in the trefoil knot (a non-trivial knot type). Notice that the disentanglement of the second conformation may be difficult [65].

system of M chains in a periodic box it suffices to measure the writhe of the M different unfoldings in order to measure the average writhe per chain in the periodic system.

Notice that the average writhe over the space of possible configurations is zero since it can take positive or negative values with the same probability. This is why we choose to study the mean absolute or the mean squared writhe in the space of configurations. The growth rate of the mean absolute writhe of (open) self-avoiding random lattice walks is equal to that of (closed) self-avoiding random lattice polygons [60, 61]. Both writhes scale as $\sim \sqrt{N}$ with chain length N. The mean squared writhe of (closed) equilateral random polygons in three dimensions scales as $\sim N$ [63]. In this paper we will be interested in the scaling of the mean absolute and the mean squared writhe of linear FENE chains in a melt, for which reference results do not exist. Chains in melts are expected to behave like ideal chains due to screening, and as $N \to \infty$, the known random walk models are expected to give similar qualitative results for the mean absolute and the mean squared writhe. We are, however, interested in the precise determination of the involved constants and prefactors of these scalings.

1. *The writhe of semiflexible linear chains*

Individual polymer chains in a melt are essentially semiflexible, that is, they assume conformations similar to those of wormlike chains with a bending angle constraint imposed (see Appendix A). The main source of semiflexibility are the excluded volume interactions between adjacent monomers. Thus, the writhe of semiflexible chains may provide useful

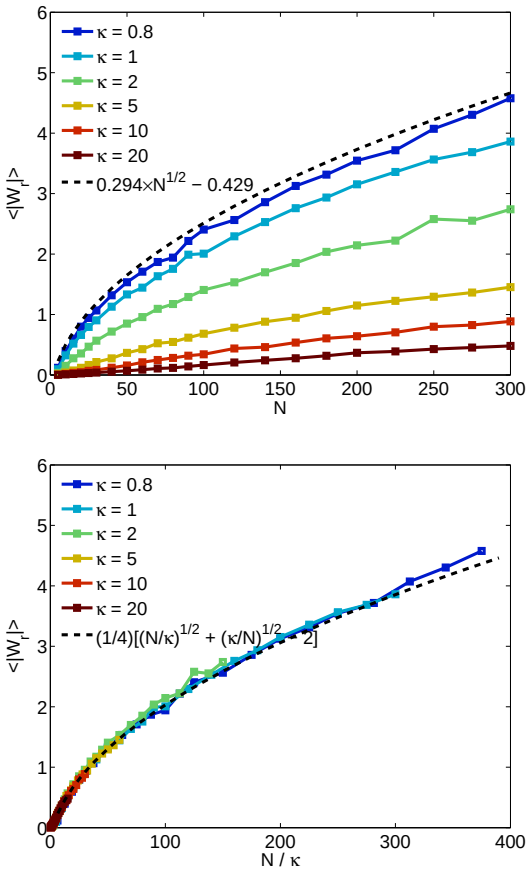

FIG. 3. (Color online) (a) Numerical results for the mean absolute writhe vs. N for various stiffness parameters κ. We include the result for an equilateral random walk, Eq. 6. (b) The same data vs. N/κ falls onto a master curve, our Eq. 4.

information for the writhe of polymer chains in a melt. Kholodenko and Vilgis [64] provided an analytic expression for the behavior of the mean squared writhe of linear semiflexible rings as a function of their stiffness parameter. Based on our numerical results, presented below, we will extend their result to linear semiflexible chains and, at the same time, to linear polymer chains in a melt. To compare these results with those for random walks we will also numerically study the mean absolute and the mean squared writhe of equilateral random walks.

Consider a *wormlike chain* (WLC), a connected linear string of $N-1$ segment unit vectors with dimensionless *stiffness parameter* κ (Appendix A). Kholodenko and Vilgis [64] proved that, for semiflexible rings, the mean absolute writhe behaves as

$$\langle |Wr| \rangle = \sqrt{\frac{\pi}{2}} \left[\left(\frac{N}{\kappa}\right)^{1/2} + \text{const} \left(\frac{N}{\kappa}\right)^{-1/2} \right], \qquad (3)$$

with an unspecified constant.

By generating linear semiflexible chains of varying κ for a range of molecular weights (Appendix A), we find that $\langle |Wr| \rangle$ is a universal function of N/κ (Fig. 3). A best fit for linear

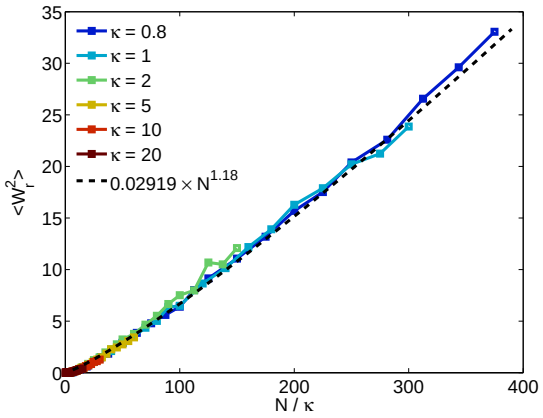

FIG. 4. (Color online) Numerical results for the squared writhe vs. N/κ for various N and stiffness parameters κ. The data falls onto a master curve, our Eq. 5.

chains turns out to be of a form very similar to the one proposed for semiflexible rings, Eq. 3. We find

$$\langle |Wr| \rangle \approx \frac{1}{5}\sqrt{\frac{\pi}{2}}\left[\left(\frac{N}{\kappa}\right)^{1/2} + \left(\frac{N}{\kappa}\right)^{-1/2} - 2\right]. \quad (4)$$

The difference, compared with the result for rings, is that we have a constant offset and a different prefactor. Our expression implies $\langle |Wr| \rangle = 0$ for $\kappa = N$. The first term in Eq. 4 dominates the typical case of $N \gg \kappa$. Notice that $1/5\sqrt{\pi/2} \approx 1/4$. For any N, the mean absolute writhe of the linear semiflexible chains is smaller than that of rings. Indeed, previous studies on the average crossing number of equilateral random walks and polygons [38, 70], on the writhe and on the self-linking number of uniform random walks and polygons in confined space [62, 71] and on the writhe of self-avoiding walks or polygons on a lattice [60, 61], indicate that the growth rate of these quantities is the same for open and closed chains but with different constants and prefactors. Similarly, shape descriptors such as the radius of gyration, the asphericity or prolateness also differ for open and closed chains of the same length [72, 73].

Similarly, we find that $\langle Wr^2 \rangle$ (Fig. 4), is very well approximated by

$$\langle Wr^2 \rangle \approx 0.02919 \left(\frac{N}{\kappa}\right)^{1.18}. \quad (5)$$

Semiflexible chains are ideal in the sense that they behave like random walks of a different step size than that of the bond length. This quantity is called the *Kuhn length*. It is therefore natural to compare our data with that of random walks that exhibit a fixed edge length and no bond angle correlation. Numerical and analytical arguments show that the mean squared writhe of closed equilateral random polygons is well described by $0.1334\,N - 0.7554$ [63]. Here, we extend this analysis to open chains. To generate equilateral random walks, each edge vector was drawn from a uniform distribution on S^2. Each data point is an average of 5000 random walks. Our numerical results on the mean absolute and the mean squared writhe, respectively, of equilateral random walks are well described by the following expressions

$$\begin{aligned} \langle |Wr_{\mathrm{RW}}| \rangle &\approx 0.294\,N^{1/2} - 0.4289, \\ \langle Wr^2_{\mathrm{RW}} \rangle &\approx 0.1084\,N - 0.95, \end{aligned} \quad (6)$$

which can be derived from Eq. 4 for $\kappa \approx 1/2$.

III. A NEW METHOD TO COMPUTE N_e-ESTIMATORS VIA WRITHE AND Z

In this section we study the number of monomers in an entanglement strand and suggest a new N_e-estimator for polymer chains in a melt. To do this, we will combine the local entanglement information, provided by the Z1 algorithm, on the number of kinks per chain with the global entanglement information given by the writhe of a chain and its primitive path.

A. N_e via writhe and Z

Let us consider a polymer chain, I, in a melt formed by $Z+1$ entanglement strands denoted as e_1, e_2, .., e_{Z+1}. The writhe of I can be expressed as (Appendix B)

$$Wr(I) = \sum_{i=1}^{Z+1} Wr(e_i) + 2\sum_{i=1}^{Z}\sum_{j=i+1}^{Z+1} L(e_i, e_j), \quad (7)$$

where $Wr(e_i)$ denotes the writhe of the entanglement strand e_i and $L(e_i, e_j)$ denotes the Gauss linking number for entanglement strands i and j. We now focus on the second summation in the right side of Eq. 7. Each term in that summation is a linking number between two entanglement strands of I. The linking number of two polymer chains before and after the application of a reduction algorithm is approximately the same [68]. Notice that the entanglement strands are polymer chains themselves. So, letting $r(e_i)$ denote the strand e_i after the reduction, we use the following approximation (see examples in Fig. 5)

$$L(e_i, e_j) \approx L(r(e_i), r(e_j)). \quad (8)$$

Notice that this approximation is valid even if the self-entanglements within an entanglement strand are neglected.

Notice next that, by definition, $r(e_i)$ must be a straight rod, and it is an edge of the primitive path that corresponds to I, PP(I). Also, by definition, the writhe of $PP(I)$ is given by

$$Wr(\mathrm{PP}(I)) = 2\sum_{i=1}^{Z}\sum_{j=i+1}^{Z+1} L(r(e_i), r(e_j)). \quad (9)$$

Based on these observations, by Eq. 8 and 9, we use the following approximation in the rest of this paper

$$Wr(\mathrm{PP}(I)) \approx 2\sum_{i<j} L(e_i, e_j). \quad (10)$$

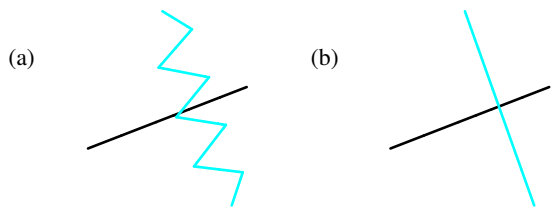

FIG. 5. (Color online) (a) Let e_1, e_2 be two entanglement strands (the black and cyan curves respectively). Their Gauss linking integral is $L(e_1, e_2) = -0.166667$. (b) Let $r(e_1), r(e_2)$ denote the corresponding reduced chains. Notice that these are the edges of the PP. Their Gauss linking integral then is $L(e_1, e_2) = -0.165372$.

Substituting Eq. 10 in Eq. 7 gives

$$\sum_{i=1}^{Z+1} Wr(e_i) = Wr(I) - Wr(\text{PP}(I)). \tag{11}$$

Notice now that

$$\begin{aligned}
&\left(\sum_{i=1}^{Z+1} Wr(e_i)\right)^2 \\
&= \sum_{i=1}^{Z+1} Wr(e_i)^2 + 2\sum_{i<j}^{Z+1} Wr(e_i)Wr(e_j) \\
&= (Z+1)\frac{\sum_{i=1}^{Z+1} Wr(e_i)^2}{Z+1} + 2\sum_{i<j}^{Z+1} Wr(e_i)Wr(e_j) \\
&= (Z+1)\langle Wr(e)^2\rangle_I + 2\sum_{i<j}^{Z+1} Wr(e_i)Wr(e_j)
\end{aligned} \tag{12}$$

where $\langle Wr(e)^2\rangle_I$ denotes the mean squared writhe of an entanglement strand in the chain I. In the following we will use the notation Wr^2 for the mean squared writhe of an entanglement strand in a fixed chain, say I, and $\mathcal{W}_e^2$ for the same quantity, averaged over all chains. Using Eqs. 11 and 12, we have

$$\begin{aligned}
&[Wr(I) - Wr(\text{PP}(I))]^2 \\
&= (Z+1)\text{Wr}^2 + 2\sum_{i<j}^{Z+1} Wr(e_i)Wr(e_j)
\end{aligned} \tag{13}$$

Thus the mean squared writhe of an entanglement strand in a given chain can be expressed as

$$\text{Wr}^2 = \frac{[Wr(I) - Wr(\text{PP}(I))]^2 - 2\sum_{i<j}^{Z+1} Wr(e_i)Wr(e_j)}{Z+1} \tag{14}$$

Taking the average over all chains then yields

$$\begin{aligned}
\mathcal{W}_e^2 = &\left\langle \frac{[Wr(I) - Wr(\text{PP}(I))]^2}{Z+1} \right\rangle \\
&-2\sum_{i<j} \left\langle \frac{Wr(e_i)Wr(e_j)}{Z+1} \right\rangle.
\end{aligned} \tag{15}$$

In this expression (Eq. 15), $Wr(I)$, $Wr(\text{PP}(I))$ and Z are known, but the $Wr(e_i), i = 1, \ldots, Z+1$ are unknown. However, one can see that the second term in the right side of Eq. 15 vanishes (Appendix C), thus $\mathcal{W}_e^2$ is given by

$$\mathcal{W}_e^2 \approx \left\langle \frac{[Wr(I) - Wr(\text{PP}(I))]^2}{Z+1} \right\rangle. \tag{16}$$

Let us now assume that the length of all the entanglement strands of chains of length N is the same, equal to $\mathcal{N}_e(N)$. Then $\mathcal{W}_e^2$ is the mean squared writhe of polymer chains of length $\mathcal{N}_e$. For polymer chains in a melt, there is a stiffness parameter κ, which can be used to represent them as semiflexible chains. Thus, the entanglement strands in the melt are also semiflexible chains with the same stiffness parameter κ. We propose to identify the mean squared writhe of an entanglement strand per chain, averaged over all chains, $\mathcal{W}_e^2$ (Eq. 16), with the mean squared writhe of semiflexible chains of length $\mathcal{N}_e$. Thus, using Eq. 5, a new N_e-estimator is given by the solution of the following equation:

$$\langle Wr^2\rangle \approx 0.02919\left(\frac{\mathcal{N}_e}{\kappa}\right)^{1.18}. \tag{17}$$

for some stiffness parameter κ that depends on the system under study. This estimator has the property that it is equal to zero for unentangled chains, that is, for chains with $Z = 0$.

B. Advantages of the new estimator

The new proposed estimator is based only on the writhe of the original and reduced chains and on Z. An innnovation of the proposed estimator is that a classical measure of topological self-entanglement of a chain, the writhe, is combined with a geometric algorithm, Z1, in order to provide physically relevant information.

Compared to the pure topological approach introduced in [30], an important advantage of this estimator is that it can be applied to systems of both linear or ring polymers (or even mixed systems), in contrast to the topological method described therein that is restricted to ring polymers. Moreover, our method can be applied to chains in any PBC model.

Compared to the pure network based approach [13], an innovation of this estimator is that it does not require knowing the locations of the kinks in the original chains nor does it require knowing L_{pp}. This is indeed important, since recent studies have pointed out the effect of *contour length fluctuation* (CLF) and *constraint release* (CR) [15, 16, 74–76] on the tube model. CLF accounts for the dynamical variation of the PP contour length of the chain with time and CR accounts for the dynamical variation of the topological constraints and

the effective tube diameter with time. These effects point out the elusive definition of an entanglement and where it applies. The new N_e-estimator does not rely directly on the criticized definition of an entanglement as a local object and may be less sensitive on CR and CLF effects. Also, in contrast to $L_{\rm pp}$ or the exact positions of the kinks in the original chains, the number of kinks per chain is captured similarly by all reduction algorithms [8]. One might expect that the writhe of the PPs which is determined by the global structure of the PP network is captured similarly by all reduction algorithms as well. Finally, the new estimator does not require a smooth set of data for its computation, as it is the case for other estimators.

Another advantage of the new N_e-estimator, is that from the analysis required for its computation, one can measure the mean and the mean squared writhe of an entanglement strand (Eq. 35 and 16, respectively) which can provide information about the self-entanglement and the conformational complexity of the polymer chains at the length scale of entanglement strands for systems in equilibrium or not.

IV. N_e- ESTIMATORS APPLIED TO FENE CHAINS

We apply the new N_e-estimator to a melt of multibead linear chains interacting via a repulsive Lennard-Jones (LJ) potential by molecular dynamics (MD) and compare our results to those obtained by other N_e-estimators for the same system. This is a classical multibead FENE chain system with a dimensionless number density 0.84 at temperature $T = 1$ [77]. We use a time step $\Delta t = 0.005$ within a velocity Verlet algorithm with temperature control. All samples were pre-equilibrated using a hybrid algorithm [78]. We apply the Z1 algorithm and compute the writhe of the chains for various molecular weights N. For short chains $N < 150$, configurations were recorded each 500 iterations (2.5 LJ time units). For $N \geq 50$, configurations were sampled each 40000 iterations (200 LJ time units). The relaxation time for FENE chains in such a melt had been estimated in [4] as $\tau \approx 0.39\, N^2 + 0.005\, N^3$, thus the recorded configurations are not uncorrelated. The MD was run a time span of the order 2τ or larger and the data was only sampled after τ to equilibrate the pre-equilibrated system.

A. Known N_e-estimators

Before computing the new N_e-estimator, we review the existing N_e-estimators and their values for the system under study.

By the application of the Z1 algorithm one obtains the kinks and the positions (beads) where they are located and from that one can estimate the average number of monomers in an entanglement strand, $\mathcal{N}_e(N)$. Notice that $\mathcal{N}_e$ can mean two different averages; it can be interpreted either as $\mathcal{N}_e^{(1)} = \langle \mathcal{N}_e \rangle_e$, where $\langle\ \rangle_e$ denotes the average over all entanglement strands in a melt, or as $\mathcal{N}_e^{(2)} = \langle\langle \mathcal{N}_e \rangle_I \rangle$, that is, the mean length of an entanglement strand per chain averaged over all chains.

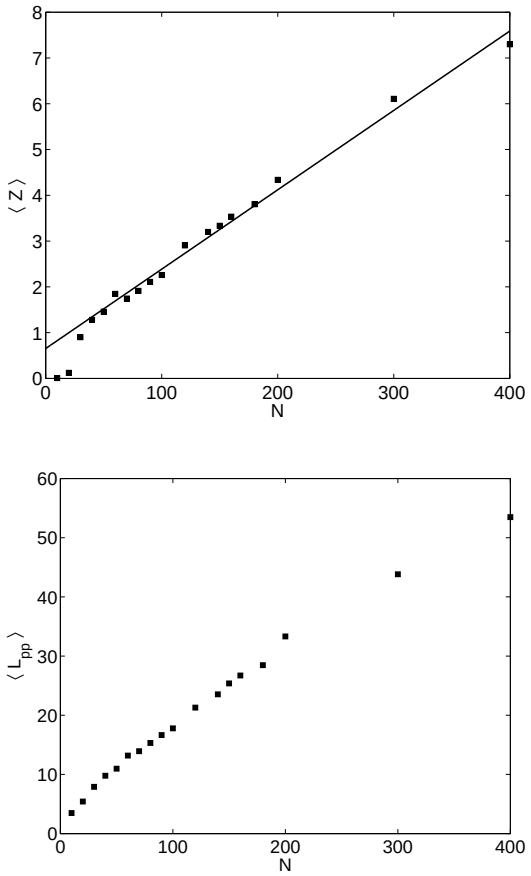

FIG. 6. (Color online) (a) Average number of kinks per chain. We observe a linear scaling with the length of the chains for $N > 40$ (Eq. 26). (b) Average contour length ($\mathcal{L}_{\rm pp}$) of the PP vs. chain length N.

Figure 7 shows the scaling of $\mathcal{N}_e^{(1)}$ and $\mathcal{N}_e^{(2)}$ as they are computed by counting beads between kinks. The two averages are different, with $\mathcal{N}_e^{(2)} \geq \mathcal{N}_e^{(1)}$. However, their difference is small, of about 5 monomers. Thus, we will refer to both averages as $\mathcal{N}_e$. Our data for $N \leq 70$ with the smallest error bars indicate a decreasing rate of growth, but the rate of convergence is slow suggesting the need to acquire more data.

The Z1 code returns values for $\mathcal{Z}$, $L_{\rm pp}$ and $R_{\rm ee}$, by which, various estimators $\mathcal{N}_e(N)$ can be computed [13]. Figure 6 shows the results for $\mathcal{Z}$ and $L_{\rm pp}$ obtained for these systems. There are estimators derived from $L_{\rm pp}$, $R_{\rm ee}$ based on a consideration of the PP as a random coil. These are the *classical S-coil* estimator

$$\mathcal{N}_e(N) = (N-1)\frac{\langle R_{\rm ee}^2 \rangle}{\langle L_{\rm pp} \rangle^2}, \tag{18}$$

the *modified S-coil* estimator

$$\mathcal{N}_e(N) = (N-1)\left(\frac{\langle L_{\rm pp}^2 \rangle}{\langle R_{\rm ee}^2 \rangle} - 1\right)^{-1}, \tag{19}$$

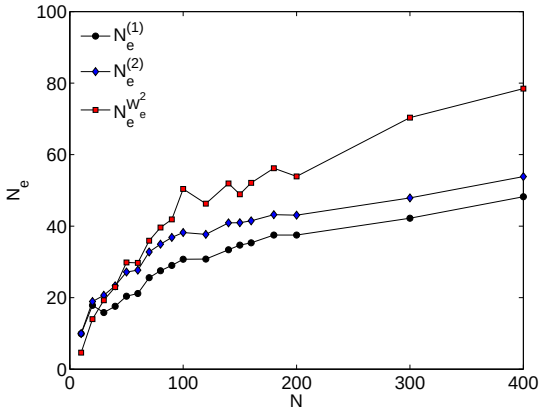

FIG. 7. (Color online) $\mathcal{N}_e(N)$ obtained by counting beads, $\mathcal{N}_e^{(1)}, \mathcal{N}_e^{(2)}$ and via writhe, $\mathcal{N}_e^{\mathcal{W}_e^2}$. We observe that $\mathcal{N}_e^{(1)}(N) := \langle\langle \mathcal{N}_e\rangle_I\rangle \approx \langle \mathcal{N}_e\rangle + 5 := \mathcal{N}_e^{(2)}(N) + 5$. Also, we observe that $\mathcal{N}_e^{\mathcal{W}_e^2}(N)$ gives a larger estimate. The data for $\mathcal{N}_e^{\mathcal{W}_e^2}(N)$ is compatible with a limiting value of $N_e \approx 80$ obtained by the M-coil estimator [13].

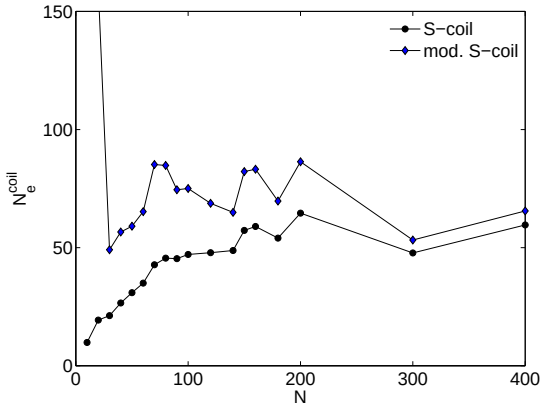

FIG. 8. (Color online) Estimators $\mathcal{N}_e(N)$ from coil properties of the PP. Both coil estimators show a convergence to a value of $N_e \approx 60$. Note that for $N = 200$ we obtain $\mathcal{N}_e^{\text{S-coil}}(200) \approx 60$ and $\mathcal{N}_e^{\text{mod. S-coil}}(200) \approx 90$, to be compared with $\mathcal{N}_e^{\text{S-coil}}(200) \approx 68$ and $\mathcal{N}_e^{\text{mod. S-coil}}(200) \approx 86.1$ [13]

.

the *M-coil* estimator

$$\left.\frac{C(x)}{x}\right|_{x=\mathcal{N}_e(N)} = \frac{d}{dN}\left(\frac{\langle L_{\text{pp}}^2\rangle}{R_{RW}^2}\right), \tag{20}$$

where $R_{RW}^2 \equiv (N-1)l_0^2$, and $C(x)$ is the characteristic ratio for a chain with x monomers. There are also estimators based on $\mathcal{Z}$, such as the *classical S-kink* estimator

$$\mathcal{N}_e(N) = \frac{N(N-1)}{N + (N-1)\mathcal{Z}}, \tag{21}$$

the *modified S-kink* estimator

$$\mathcal{N}_e(N) = \frac{N}{\mathcal{Z}}, \tag{22}$$

and the *M-kink* estimator

$$\frac{1}{\mathcal{N}_e(N)} = \frac{d\mathcal{Z}}{dN}. \tag{23}$$

The nomenclature had been overtaken from [13].

Our data for chains of length $N > 100$ is not smooth enough to use the M-coil and M-kink estimators, as these use the slopes of $\mathcal{Z}$ against N. These had been estimated for the same type of systems in [13]. The authors reported $N_e \approx 46$ and $N_e \approx 85$ from the M-kink and M-coil estimators respectively. The simpler S-coil and S-kink estimators are shown in Figs. 8 and 9, and lead to $N_e \approx 60$ and $N_e \approx 50$, respectively. The value of N_e from rheological studies for the same systems is $N_e \approx 75$ [12].

The challenge that remains is to find an estimator that better approximates the N_e values determined in experiments. As it was pointed out in [13] the classical estimators tend to underestimate N_e. On the other hand, the modified estimators tend to overestimate N_e for weakly entangled systems.

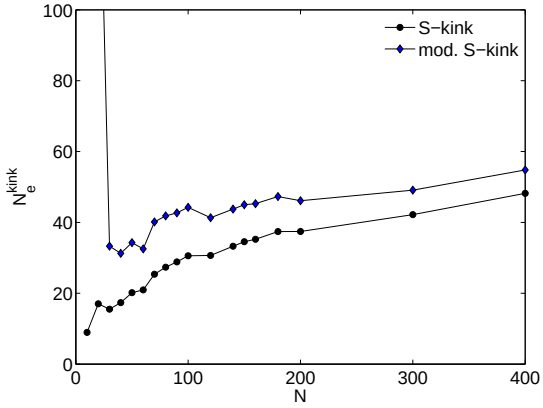

FIG. 9. (Color online) Estimator $\mathcal{N}_e(N)$ based on the average number of kinks per chain, $\mathcal{Z}$. Both kink estimators show a convergence to a value of $N_e \approx 50$, well in accord with $N_e \approx 48.9$ [13]. Note that for $N = 200$ we obtain $\mathcal{N}_e^{\text{S-kink}}(200) \approx 35$ and $\mathcal{N}_e^{\text{mod. S-kink}}(200) \approx 45$ ro be compared with $\mathcal{N}_e^{\text{S-kink}}(200) \approx 40$ and $\mathcal{N}_e^{\text{mod. S-kink}}(200) \approx 45$ [13].

An *ideal* estimator $\mathcal{N}_e(N)$ is one that it correctly predicts N_e for $N \geq N_e$ and approaches N_e as $N \to N_e$. Thus, the S-estimators are not ideal. On the other hand, the M-estimators are nearly ideal, since they converge faster than the S-estimators.

We note that the M-estimators, based on kinks, give an N_e value almost half the one obtained from the estimators based on coils ($N_e \approx 46$ and $N_e \approx 85$ respectively). Similar discrepancies have been encountered before [9, 79–81], and this difference has been explained by suggesting that there exist directional correlations between entanglement strands along the same PP which decay exponentially with distance. That is, PP conformations are not RWs at the length scale defined

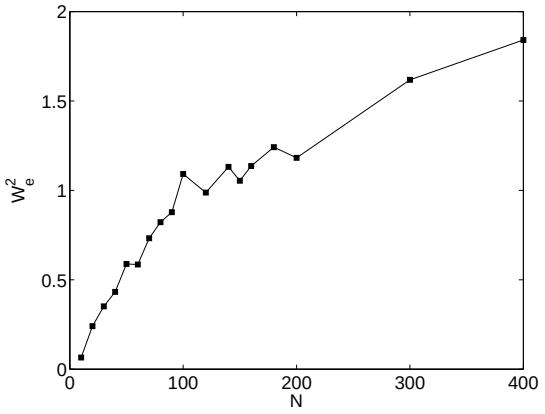

FIG. 10. The average mean squared writhe of an entanglement strand in a chain over all chains, $\mathcal{W}_e^2 = \langle \mathrm{Wr}^2 \rangle$ computed by Eq. 16. This is the average variance of the writhe of an entanglement strand in a chain over all chains. The data suggest that $\mathcal{W}_e^2$ approaches an asymptotic value of approximately 2.

by the distance between kinks, a fact that is also supported by our numerical results in Section V C. It is worth noting that these considerations do not yield much information about the distribution of the lengths of entanglement strands. The probability distribution of individual $\mathcal{N}_e = N/\mathcal{Z}$ values obtained for a single chain is shown to be (Appendix D)

$$P(\mathcal{N}_e) = \frac{N\mu^{N/\mathcal{N}_e - 1} e^{-\mu}}{\mathcal{N}_e^2 \Gamma(N/\mathcal{N}_e)}. \tag{24}$$

where $\Gamma(x)$ is the Gamma function. This implies that maybe neither of the two versions may be entirely correct.

B. The new N_e-estimator using Z1 and writhe

The new N_e-estimator will be computed by the general formula of Eq. 17. For linear FENE chains in a melt, one has $\langle R_{\mathrm{ee}}^2 \rangle \approx Nb^2 = Nl_p b_0$ with $b = 1.34 b_0$, where $b_0 \approx 0.97$ is the bond length. Thus the persistence length is $l_p \approx 1.85 b_0 \approx 1.90$ and the Kuhn length is $l_K \approx 2l_p \approx 3.80$. The corresponding stiffness parameter is $\kappa \approx 2.34$ as obtained from the exact relationship $\coth(\kappa) - \kappa^{-1} = \exp(-l_p^{-1})$ (see Appendix A). Thus, using Eq. 17, a new N_e-estimator for linear FENE chains in a melt is given by the solution of the following equation

$$\mathcal{W}_e^2(N) = 0.0107\, \mathcal{N}_e^{1.18}(N). \tag{25}$$

From the values of the writhe of the original and reduced chains (shown in Fig. 12), and by $\mathcal{Z}$, we can compute the mean squared writhe of an entanglement strand, $\mathcal{W}_e^2$ (Eq. 16). Figure 10 shows the values of $\mathcal{W}_e^2$ for our data.

Using the data of $\mathcal{W}_e^2$ for linear FENE chains of various molecular weights shown in Fig. 10, we obtain the values of $\mathcal{N}_e(N)$ shown in Fig. 7. Let us denote this estimator by $\mathcal{N}_e^{\mathcal{W}_e^2}$. The data suggests a limiting value of $N_e \approx 80$. This limiting value agrees with the known N_e value reported in experiments [12, 14].

We observe that for $N \leq 40$, the values of $\mathcal{N}_e^{\mathcal{W}_e^2}$ are close to those obtained by counting beads between entanglements, but $\mathcal{N}_e^{\mathcal{W}_e^2}$ becomes strictly larger for $N > 40$. For $100 \leq N \leq 70$, $\mathcal{N}_e^{\text{S-kink}} \leq \mathcal{N}_e^{\mathcal{W}_e^2} \leq \mathcal{N}_e^{\text{S-coil}}$ but for $N > 250$, $\mathcal{N}_e^{\mathcal{W}_e^2}$ is larger than all S-estimators. As N increases, $\mathcal{N}_e^{\mathcal{W}_e^2}(N)$ increases as well, reaching values that are consistent with the N_e values obtained from rheological studies, that is, $\mathcal{N}_e(N) \approx 70$ for $N = 350$ [14]. We notice that $\mathcal{N}_e^{\mathcal{W}_e^2}$ is not an ideal estimator, since it converges quite slowly. However, it approaches the M-coil estimator faster than any of the other estimators. This indicates that $\mathcal{N}_e^{\mathcal{W}_e^2}$ could be used to approximate the $\mathcal{N}_e^{\text{M-coil}}$ estimator for a non smooth set of data.

From the mean absolute writhe of the original chains (see Fig. 12(a), we observe that $\langle |Wr| \rangle \geq 1$ for $N \geq 80$, which indicates that, on average, these long chains with $N \geq 80$ contain knots [63], in the sense that a random closure of the chains would result in a non-trivial knot type [35, 36]. In other words, the value of N_e predicted by $\mathcal{N}_e^{\mathcal{W}_e^2}$ may be the result of a change in the topology of the chains. We note that the estimates of N_e based on counting the number of beads or the M-kink estimators give an estimate $N_e \approx 45$ that is almost half of the one reported by using topological/geometrical methods or rheological experiments [9, 13, 80, 81]. The observed crossover in the scaling of $\mathcal{Z}$ at $N \approx 45$ (see Section V A) indicates the transition to the presence of kinks for chains with $N > 45$. These findings suggest that N_e is related to the global topological entanglement of the chains, while only a fraction of this value, approximately half, seems to be related to the number of local obstacles restricting the local motion of the chains.

V. DISCUSSION: Z1 AND WRITHE ANALYSIS OF LINEAR FENE CHAINS IN A MELT

In this section we discuss additional results on $\mathcal{Z}$ and writhe that stem from our analysis of N_e for linear FENE chains in a melt. More precisely, in this section we focus on our system of linear FENE chains and discuss Z, the writhe of the original and reduced chains and the mean and mean squared writhe of the entanglement strands. All these measures can provide further insight on the entanglement of linear FENE chains in a melt.

A. The average number of TCs (kinks) per chain

In Fig. 6(a) the value of $\mathcal{Z}$ is shown for various chain lengths N. Our result is in agreement with previous studies which predict a linear scaling of $\mathcal{Z}$ with N [7, 8]. A linear fit of our $N > 40$ data yields

$$\mathcal{Z} = 0.0173\, N + 0.679. \tag{26}$$

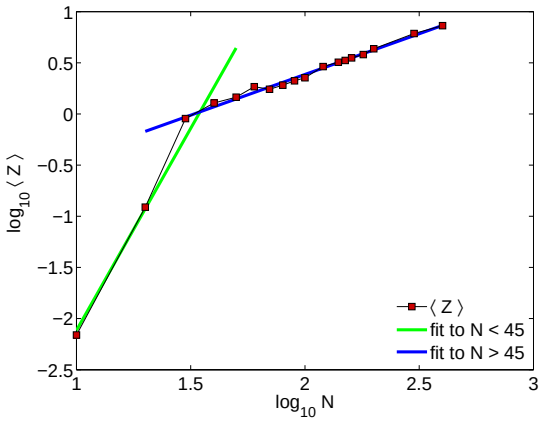

FIG. 11. (Color online) Average number of kinks per chain with the length of the chains in double-logarithmic representation reveals a crossover at $N \approx 45$, that finds its analogue in the writhe of the PPs.

compared with $\mathcal{Z} \approx 0.02\,N - 0.14$ [13]. We observe that $\mathcal{Z} \approx 0$ for $N \leq 20$, indicating that kinks cannot be formed below a certain threshold length. Also, $\mathcal{Z} > 1$ for $N > 30$. Since the variance of $\mathcal{Z}$ is of the same order as $\mathcal{Z}$ [15, 66], the error mean of $\mathcal{Z}$, er_Z, of a sample of C independent polymer melt configurations is $er_Z = \sqrt{\mathcal{Z}/C} \approx 0.1\,\sqrt{N/C}$. Thus, for our systems of $N < 400$ ($C > 100$), we obtain $er_Z < 0.2$, small compared with the values of $\mathcal{Z}$. Figure 11 shows the data of Fig. 6(a) in double logarithmic representation. We clearly observe a crossover at about $N \approx 45$ where $\mathcal{Z} \approx 2$. This may indicate that chains of $N < 45$ are only weakly entangled, and that the value $\mathcal{Z} = 2$ serves to mark the transition to the asymptotic linear behavior. Figure 6(b) shows the average contour length $\mathcal{L}_{\rm pp}$ of the PP that increases linearly with N, in agreement with earlier works [13].

B. The writhe of linear FENE chains in a melt

In Section II B 1 we show that the mean absolute writhe of semiflexible chains of length N and stiffness κ can be approximated by Eq. 4. Thus, for an individual linear FENE chain embedded in a melt, which corresponds to a semiflexible chain of $\kappa \approx 2.34$, we have (for $N > 2$)

$$\langle |Wr| \rangle \approx 0.1638\,N^{1/2} + 0.383\,N^{-1/2} - 0.5013. \qquad (27)$$

This is in good agreement with the measured data shown in Fig. 12(a). In the same Figure we show data for the mean absolute writhe of the corresponding PPs.

It is interesting to notice that the average writhe in a dense system of flexible chains with excluded volume fits the general scaling of that of a WLC without excluded volume. Recall that the writhe is a measure of global self-entanglement (or complexity) of a fixed configuration of one chain. This suggests that an individual chain in the melt, on average, assumes a similar configuration as a semiflexible chain in the vacuum with stiffness parameter defined by the chain in the

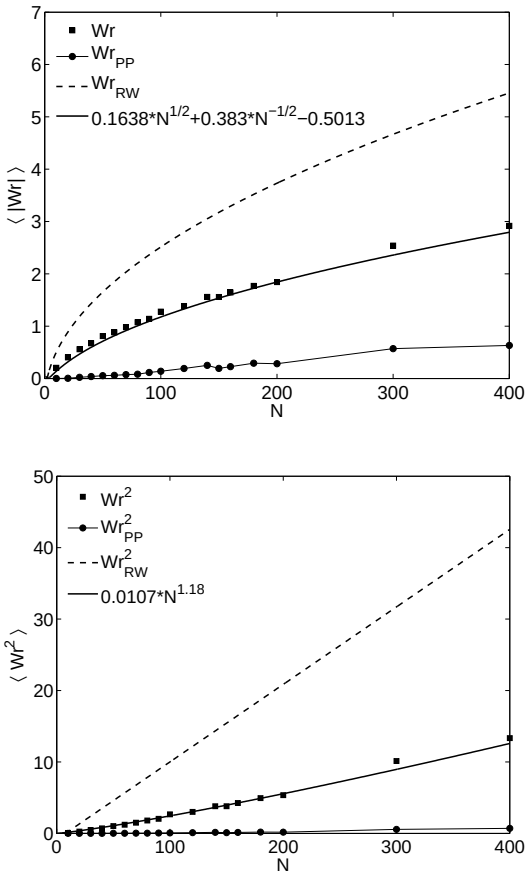

FIG. 12. (a) The average absolute writhe of (i) linear FENE chains in a melt (squares) and (ii) their PPs (circles). The black curve is the predicted scaling for individual semiflexible chains (Eq. 27). We notice that for $N > 80$, $\langle |Wr| \rangle > 1$. The dotted black curve is the scaling for equilateral RWs (Eq. 6), which much deviates from that of the flexible FENE chains and their PPs. (b) Same as above for the squared writhe. Mean squared writhe of linear FENE chains (squares) and their PPs (circles). The black line shows the scaling for semiflexible chains (Eq. 29). The dotted black line shows the scaling for equilateral RWs (Eq. 6) for comparison.

melt. Notice that this does not imply any relation of the two systems with respect to entanglements (kinks). Indeed, the FENE chains in a melt are entangled with each other, but chains in the vacuum are not entangled with others. The effect of the presence of other chains is intrinsically captured by the stiffness parameter $\kappa \approx 2.34$ which determines the writhe of the chains in a melt. Moreover, the l_p values suggest that the FENE chains of length N behave like random walks of length $N/4$, also supported by our data shown in Fig. 12(a).

The writhe and the number of kinks in a chain are not related in general, since a chain (in the original state) with $Z = 0$ (in its reduced state) may have the same writhe with a chain with $Z \neq 0$. However, in a system for which we know that $\mathcal{Z} \neq 0$, it makes sense to examine if there exists a relation between $\mathcal{Z}$ and $\langle |Wr| \rangle$. Figure 13 shows the scaling of the mean absolute writhe of a chain with respect to the av-

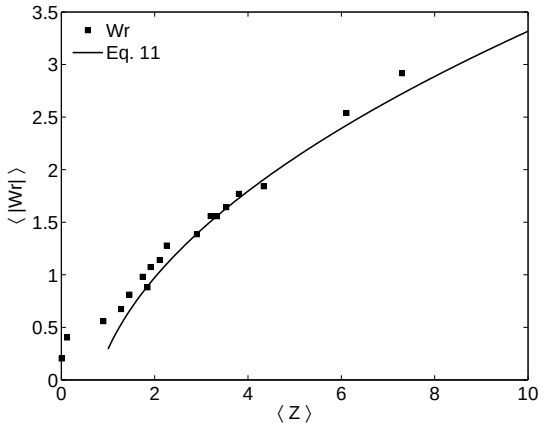

FIG. 13. The mean absolute writhe of a chain vs. the average number of kinks per PP. Interestingly, the writhe of the individual chain in a melt seems to be related to the number of kinks in a multi-chain system, connecting thus local and global entanglement properties. Because the relationship is bijective, there is a one-to-one correspondence, which seems linear at first glance, but is expected to be better described by Eq. 28 for large $\mathcal{Z}$.

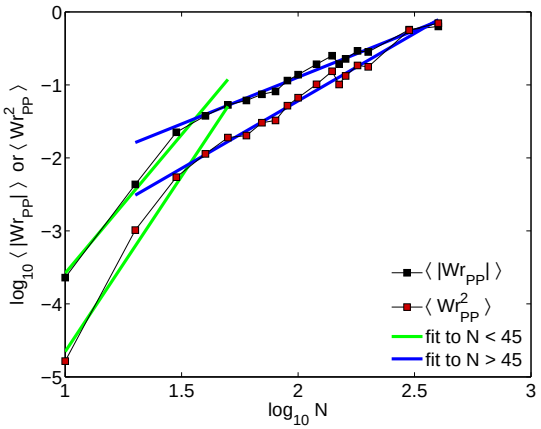

FIG. 14. (Color online) Double-logarithmic plot of the mean absolute writhe and of the mean squared writhe of the PPs. The different scaling with respect to N appears as a crossover (doubling slope) at about $N \approx 45$.

erage number of kinks per chain for the system under study. Combining Eq. 26 and Eq. 27 we see that, for $N > 40$, for linear FENE chains in a melt $\langle |Wr| \rangle$ and $\mathcal{Z}$ should be related as follows:

$$\begin{aligned}\langle |Wr| \rangle \approx\ & 1.245\,(\mathcal{Z} - 0.679)^{0.5} \\ & + 0.0504\,(\mathcal{Z} - 0.679)^{-0.5} - 0.5013.\end{aligned} \tag{28}$$

Notice that Eq. 28 is based on the linear scaling of $\mathcal{Z}$ (for $N > 40$) and on Eq. 27. The linear scaling of $\mathcal{Z}$ has been confirmed by many studies [13, 15, 66] and Eq. 27 follows the form derived analytically by Kholodenko and Vilgis. This implies that, for this system, local and global entanglement properties of the chains may be related. We note that a relationship between the number of kinks in a system of freely jointed chains of tangent hard spheres and the probability of knotting has been proposed. Specifically, it is conjectured that the population of entanglements and knots follow the same scaling laws at all volume fractions [29, 34]. Using Eq. 28 we can estimate $\mathcal{Z}$ from writhe or the inverse. Thus, for this system, we can compute N_e-estimators involving $\mathcal{Z}$ by computing the writhe of only a subcollection of chains.

For the mean squared writhe, following the previous discussion (Section II B 1), for a FENE melt we have

$$\langle Wr^2 \rangle \approx 0.0107\, N^{1.18}. \tag{29}$$

This is captured by the data shown in Fig. 12(b) for the mean squared writhe of a polymer chain. In the same figure we show data for the mean squared writhe of the corresponding PPs. Notice that $\langle Wr^2 \rangle = \mathrm{Var}(Wr)$, since $\langle Wr \rangle = 0$. The black curve shows the scaling of the mean squared withe of FENE chains from Eq. 29 and the dotted black line shows the scaling of the corresponding equilateral random walks. Again, the values of the polymer chains are much smaller than those of random walks, as is now expected. From the variance of Wr, we can compute the error of its sample mean, er_{Wr}. For a sample size of C melt configurations of M chains each, $er_{Wr} = \sqrt{\langle Wr^2 \rangle / CM} = 0.1\, N^{0.59}/\sqrt{CM}$. Upon analyzing $C = 100$ independent configurations with $M = 100$ chains of length $N < 400$, the error $er_{Wr} < 0.004$ is small compared to the reported values of Wr.

C. The writhe of the primitive path

For a melt of ring polymers, if two chains are linked, the same must be true for the two corresponding PPs, if self-crossings are not allowed. Even the link type of the PPs must be the same as that of the closed chains and consequently, their linking number is the same. Similarly, the knot type of both chains is the same as the knot types of their PP. But, the conformation differs significantly between a chain with $N-1$ steps and its PP. The PP, as it is obtained by the Z1 algorithm, also is a polygonal chain, but with a reduced number of steps, $\mathcal{Z}+1$, and an increased average edge length. Even in the case of ring polymers, the writhe of each chain changes. In the case of linear polymers, both the linking number and the writhe of the chains will change continuously under the deformation of the chains. We note, however, that the effect of the reduction may differ for each measure. More precisely, the reduction respects the entanglements (kinks), which have an important impact on the linking integral of the two chains, but each chain becomes locally linear, which may have an important impact on the writhe of each chain. Numerical results, [68], show that the linking integral of two chains is almost the same before and after the reduction.

The writhe of the PP is a quantity that characterizes the global geometrical/topological complexity of the PP. It is therefore of particular interest to compare it to that of the original chain and to that of a random coil. Moreover, the writhe

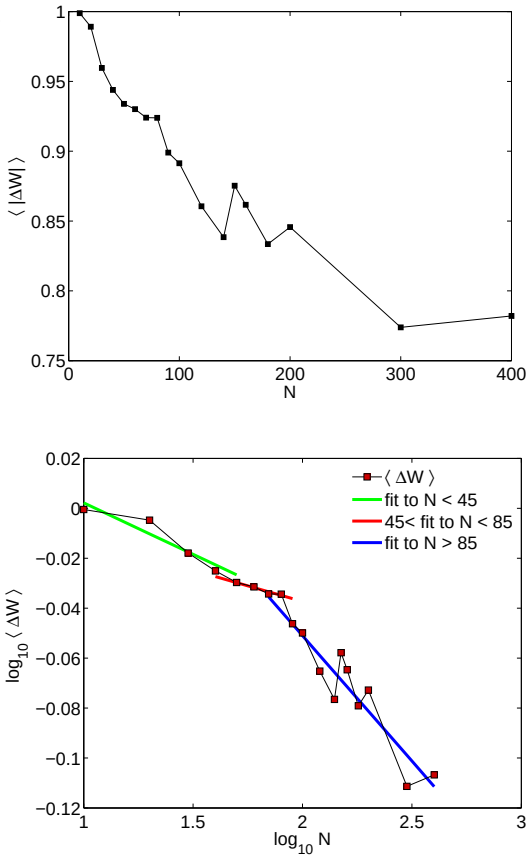

FIG. 15. (Color online) (a) The normalized mean absolute difference of the writhe between the original and reduced chains, $|\Delta\mathcal{W}| = |Wr - Wr_{\rm PP}|/|Wr|$. (b) Double logarithmic representation of the same data reveals moderate changes in slope at about $N = 45$ and $N = 80$.

of the PP in addition to Z, could provide further information on the nature of the kinks in a chain. For example, let us consider a configuration of a reduced chain with $Z \neq 0$, but whose kinks correspond to small bending angles. Its writhe will be approximately zero. If the bending angles of the kinks are large, as is usually the case for knotted arcs, then its writhe will be larger (see Fig. 2 for an illustrative example). Thus, the writhe of the PP could provide information about the nature of the kinks, and the so-called *persistent* entanglements [65].

Figure 12 shows the scaling of the mean absolute and the mean squared writhe of a PP as a function of N and Fig. 14 shows the corresponding double logarithmic plots. Both quantities show a crossover at $N \approx 45$. A crossover at $N \approx 45$ appeared also for the scaling of $\mathcal{Z}$. Thus, one should expect that this would also affect the writhe of the PPs. For $N \geq 45$, the data is fitted to the function

$$\begin{aligned} \langle |Wr_{\rm PP}| \rangle &= 0.006\, N^{0.8} - 0.127, \\ \langle Wr^2_{\rm PP} \rangle &= 0.000065\, N^{1.56274} - 0.0244619. \end{aligned} \tag{30}$$

We observe that the writhe of the PP is smaller than the

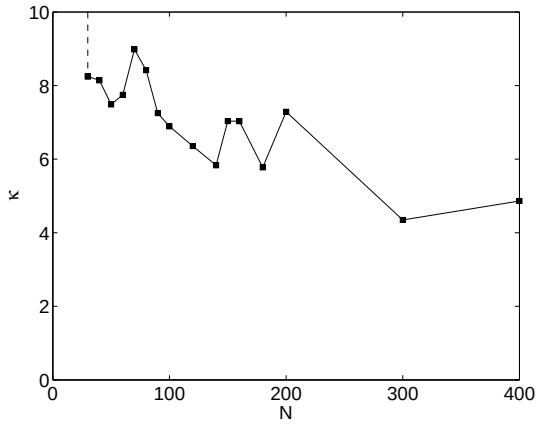

FIG. 16. Stiffness parameter κ assigned to PPs by identification with the WLC chain model. We notice that κ diminishes, as the chains get longer, thus, the PP cannot be identified with a semiflexible chain of constant κ over the range of chain lengths studied.

writhe of the original chains. The normalized mean absolute difference between the writhe of the original and reduced chains, $|\Delta\mathcal{W}| = (|Wr - Wr_{\rm PP}|)/|Wr|$ is shown in Fig. 15(a). Figure 15(b) shows the corresponding double logarithmic plot. There might be a crossover at $N \approx 45$ that is related to the previously mentioned crossover of $\langle |Wr_{\rm PP}| \rangle$ at the same N. Clearly, there is a crossover at $N \approx 80$, where the relative difference decreases at a faster rate. Note that for $N \geq 80$, $\langle |Wr| \rangle \geq 1$ which suggests that the chains of that length on average contain knots. Moreover, our estimate of $\mathcal{N}_e \approx 80$ provides further support for the entanglement of the chains. This crossover indicates that once the chains are entangled, there is a larger portion of the writhe of the original chains that remains in the PP. This transition could also be related to a change in the nature of the kinks with an increased presence of those with larger bending angles, and thus to the presence of persistent entanglements.

Edwards proposed that the PP behaves as a random coil [1]. From this viewpoint, the PP is also characterized by some persistence length that we may evaluate. One possible approach to estimating l_p for the PP is to inspect the squared end-to-end $\langle R^2_{\rm ee} \rangle$ values, and compare these values with the formula for the WLC with $L = \mathcal{Z} + 1$ segments of identical length (Appendix A). This yields a dimensionless l_p for the PP and dimensionless κ via Eq. A3. Using this method, we evaluate κ at each length. Indeed, for $N = 10$ and $N = 20$, the reduced chains are in general straight rods, since there are no entanglements, and $l_p \to \infty$, as expected for very stiff chains. For $N > 20$ the values of l_p result, via Eq. A3, in the values of κ that are shown in Fig. 16. It is clear that the PPs are not random walks. However, we observe that, as N increases, κ decreases, thus we cannot exclude the possibility that the PPs are well described by WLC's with $\kappa \to 0$ (random walks) as $N \to \infty$.

For all molecular weights observed in this study, the values of the writhe of the PP are small, consistent with what one would expect for a random coil of that length, ie. with $\mathcal{Z} + 1$

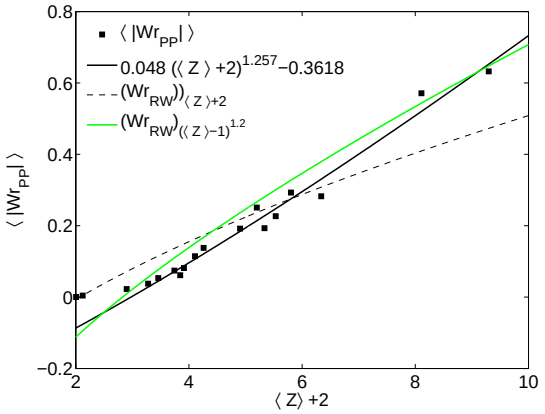

FIG. 17. (Color online) The mean absolute writhe of the primitive path as a function of the number of segments in a PP. The black curve shows the best fit for the mean absolute writhe of the PP (Eq. 31) and the dotted black curve shows the writhe of RWs of the same number of steps (Eq. 33), i.e. $\mathcal{Z}+1$. We notice that the mean absolute writhe of the PPs is not that of RWs of $\mathcal{Z}+1$ edges.

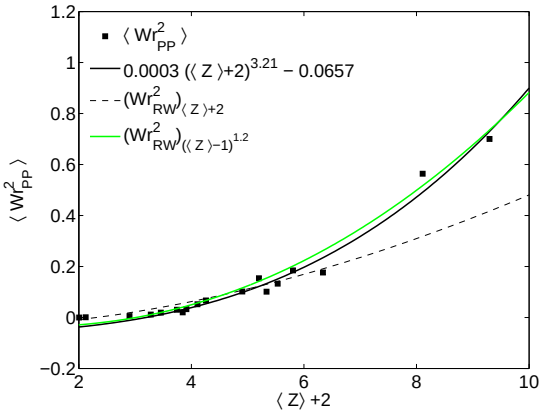

FIG. 18. (Color online) The mean squared writhe of the primitive path as a function of the number of segments in a PP. The black curve shows the best fit for the mean squared writhe of the PP (Eq. 32) and the dotted black curve shows the mean squared writhe of RWs of the same number of steps (Eq. 34), i.e. $\mathcal{Z}+1$. We notice that the mean squared writhe of the PPs is not that of RWs of $\mathcal{Z}+1$ edges.

edges. In order to compare the behavior of the PPs with that of semiflexible chains, we will compare their writhes. To do this, we make the following approximations: first, we fix the stiffness parameter equal to its average value over all molecular weights; second, we let the number of steps of the PPs equal to $\mathcal{Z}+1$, for all PPs that correspond to original chains of length N; and third, we let the edge length of a PP to be equal to N_e for all PPs. For our data, the average stiffness of the PPs is $\kappa \approx 6.9$. This is clearly a different value than that of the FENE chains, or that of random walks. It indicates that the PP is much stiffer in terms of the length scale over which orientation correlations are lost. Note that the bending angles might be actually larger than those of a FENE chain with excluded volume. Then, for this average κ, and for $N = \mathcal{Z}+2$, Eq. 27 gives different values for $\langle|Wr_{\rm PP}|\rangle$. The data for the PP are best fitted to a function of the form

$$\langle|Wr_{\rm PP}|\rangle \approx 0.048\,(\mathcal{Z}+2)^{1.257} - 0.3618. \qquad (31)$$

Similarly, for $\kappa \approx 6.9$, the data of the mean squared writhe are best fitted to the function

$$\langle Wr^2_{\rm PP}\rangle \approx 0.1635\left(\frac{\mathcal{Z}+2}{\kappa}\right)^{3.21} - 0.0657. \qquad (32)$$

From this analysis of $\langle|Wr_{\rm PP}|\rangle$ and $\langle Wr^2_{\rm PP}\rangle$, we see that the PP cannot be modeled by semiflexible chains. A reason why one might expect a different scaling for the PP is because, at least for the data under consideration, the number of steps in a PP, as defined by $\mathcal{Z}$ is very small and may not be comparable to the data presented in Section II B 1 which concern chains of length $N \geq 10$. In fact, for $N \leq 400$, we get $\mathcal{Z}+2 \leq 10$. By generating equilateral random walks of length $N \leq 10$, the best fits of the mean absolute writhe and the mean squared writhe are

$$\langle|Wr_{\rm RW}|\rangle \approx 0.1986\,N^{0.62} - 0.311, \qquad (33)$$
$$\langle Wr^2_{\rm RW}\rangle \approx 0.0082\,N^{1.79} - 0.037, \qquad (34)$$

respectively, different than those for $N \geq 10$. These are shown with the dotted black curve in Figs. 17 and 18 respectively. We note that the writhe of the PPs becomes larger than the writhe of the RWs for $\mathcal{Z}+2 > 5$, which corresponds to the original chains of length $N > 150$. This suggests that the writhe of the PPs may be better compared to that of RWs of more than $\mathcal{Z}+1$ steps. (The green lines in Figs. 17 and 18 show the mean absolute and the mean squared writhe of equilateral random walks of $(\mathcal{Z}-1)^{1.2}$ vertices for comparison.)

D. The writhe of an entanglement strand

The *entanglement strand*, a part of the polymer chain of N_e monomers, is essential in the tube model. It determines a lengthscale at which a crossover from Rouse to reptation dynamics occurs. Therefore, it is of particular interest to examine the conformational properties of the chains at the lengthscale of the entanglement strands. In this section, based on the method presented in Section III to estimate N_e, we derive semi-analytic formulae for the mean absolute and the mean squared writhe of an entanglement strand. These quantities are measured for the first time and are expected to provide information about the self-entanglement and the conformational complexity of the polymer chains at the length scale of entanglement strands.

1. The mean writhe of an entanglement strand in a chain

The analysis in section III allows us to compute the mean writhe of an entanglement strand in a chain from Eq. 11 as

$$\begin{aligned} \mathrm{Wr} &= \frac{\sum_{i=1}^{Z+1} Wr(e_i)}{Z+1} \\ &= \frac{Wr - Wr(\mathrm{PP})}{Z+1} \end{aligned} \tag{35}$$

where Wr denotes the writhe of the original chain and $Wr(\mathrm{PP})$ denotes the writhe of its PP. This formula for Wr is semianalytic. For its derivation the only approximation used is the one described by Eq. 10. Thus, by Eq. 35 we can compute Wr, using only the writhe of the original and reduced chains and the number of kinks, without having to define directly the exact locations of the entanglement strands in a chain. The entanglement strands are defined only indirectly by using the Z1 reduced chain as the PP of a chain in a melt and from that computing the writhe of the PP.

Note that the writhe of an entanglement strand in a chain can take positive or negative values with the same probability. Thus, taking its average over all entanglement strands in the same chain, ie. Wr will be approximately zero for a sufficiently long chain. For moderate molecular weights, that are the most common in numerical studies, Wr, may be non-zero because the number of entanglement strands in the chain, ie. $Z+1$, may be small. Also, Wr will take both positive and negative values with the same probability, thus the mean writhe of an entanglement strand in a chain, averaged over all chains, is zero. For this reason, we will be interested in the value of the absolute value of the mean writhe of an entanglement strand in a chain, averaged over all chains, $\langle|\mathrm{Wr}|\rangle$ that can be derived from Eq. 35. In the following we will denote $\langle|\mathrm{Wr}|\rangle$ by $\mathcal{W}_e$.

Fig. 19 shows the values of $\mathcal{W}_e$ for our systems of linear FENE chains in a melt. The data suggest that $\mathcal{W}_e$ reaches an asymptotic value of approximately 0.4. It is interesting to note that even though the longer chains contain more entanglement strands, their mean writhe does not vanish.

2. The mean squared writhe of an entanglement strand in a chain

Since the mean writhe of an entanglement strand in a chain is approximately equal to zero for very long chains, one would prefer to study the mean absolute writhe of an entanglement strand in a chain, averaged over all chains. Unfortunately, this is very difficult to accomplish. Following the analysis presented in Section III, we can measure the average, over all chains, of the mean squared writhe of an entanglement strand in a chain by using Eq. 16. Since $\langle\mathrm{Wr}\rangle \approx 0$, $\mathcal{W}_e^2$ is the average variance of the writhe of an entanglement strand in a chain over all chains, that is $\mathcal{W}_e^2 \approx \langle\mathrm{Var}(Wr(e))\rangle$. We note that Eq. 16 gives a semi-analytic formula for $\mathcal{W}_e^2 \approx \langle\mathrm{Var}(Wr(e))\rangle$. So, again, we can compute the average variance of the writhe of an entanglement strand without defining the locations of the entanglement strands in a chain, by using only Z and the writhe of the original and reduced chains.

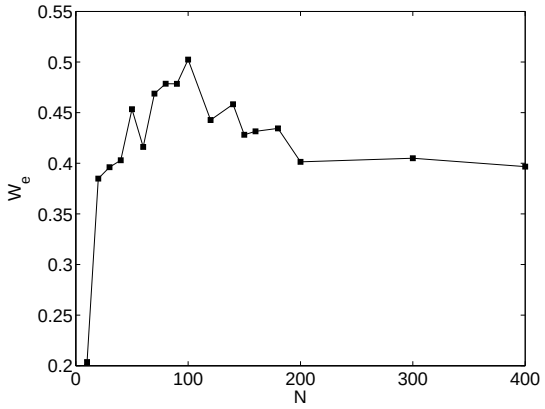

FIG. 19. The average absolute mean writhe of an entanglement strand in a chain over all chains in a melt, $\mathcal{W}_e = \langle|\mathrm{Wr}|\rangle$. It approaches an asymptotic value different than zero, as expected for an average over a sample of random coils of the same length. This may be related to the variance of the length of the entanglement strands in a chain.

Figure 10 shows the values of $\mathcal{W}_e^2$ for our data. We observe that $\mathcal{W}_e^2$ seems to converge to an asymptotic value of approximately 2, which is consistent with the value of $\langle Wr^2\rangle = 1.88$ for chains of length $N = 80$, as expected by our estimate of $N_e \approx 80$, computed in Section IV B for this system. We observe that $\mathcal{W}_e^2 > 1$ for $N > 95$. This suggests the existence of entanglement strands with absolute writhe larger than one for long chains. Note that the chains of length $N > 95$ contain on average one entanglement strand of length $N_e \approx 80$. This suggests that once entanglement strands are formed, there are probably some, on average, that contain knots. Note that knotted arcs at the length scale of N_e suggest the presence of self-entanglements in the reduced chains, since there is a large probability that no other chain interpenetrates. Interestingly, we arrive at the same result that was pointed out in [14]: Self-entanglements concerns local knotting or, more precisely, knotted arcs are likely to occur at the length scale of the entanglement strands.

VI. CONCLUSIONS

In this study, the writhe, a global measure of self-entanglement of a chain, and $\mathcal{Z}$, the number of kinks in the PP network for a multichain polymer melt configuration, are used to define a new estimator of N_e, the number of monomers in an entanglement strand, via Eq. 25. An advantage of this estimator is that it is valid for both open and closed chains in any PBC model. Moreover, it does not depend directly on the exact locations where the kinks occur, nor on the value of L_{pp}. We have applied our method to linear FENE chains in a melt in equilibrium conditions. Our estimate $\mathcal{N}_e \approx 80$ is in good agreement with values reported from experiments. This provides strong evidence that the combination of local and global entanglement measures can provide information that is rele-

vant to the study of entanglement in polymers. By comparing our estimator with previous estimators, we observe that it converges faster than the S-estimators. Another strength of this estimator is that it does not rely on a smooth set of data for various molecular weights as required by the M-kink estimator to unambiguously calculate numerical derivatives.

In the coarse of developing the estimator we numerically studied the mean absolute and the mean squared writhe of linear semiflexible chains. Our numerical results suggest a scaling similar to the analytical prediction of Kholodenko and Vilgis for semiflexible ring polymers, Eq. 4. Focusing on linear FENE chains in a melt in equilibrium conditions, our results suggest a relation of the form described by Eq. 27 for the mean absolute writhe. This result confirms that the polymer chains in a melt have characteristics similar to those of semiflexible chains in the vacuum with a stiffness parameter determined by the system. For our systems of linear FENE chains in a melt, we observe that $\mathcal{Z}$ and the writhe of the chains are related by Eq. 28. Although, this is not a general result, it is of interest since, at first glance, one might expect these quantities to be unrelated because they capture different entanglement information. Also, the average number of kinks per chain, $\mathcal{Z}$, is computed from the Z1 reduced chains, while the writhe of a chain concerns a frozen initial configuration of a chain in a melt.

Our numerical results show that the writhe of the Z1 reduced chains is significantly altered and that it is not comparable to that of semiflexible chains or random walks, indicating that the bending angles of the PPs are larger. From the analysis of $\mathcal{Z}$ and the difference of the writhe of the original and reduced chains, we observe two different crossovers in their scalings, at $N \approx 45$, which indicates the presence of kinks, and at $N \approx 80$, respectively, which indicates that the system is topologically entangled. This finding suggests a possible explanation for the discrepancies between the different N_e-estimators.

Finally, we provide a semi-analytical expression for the mean and the mean squared writhe of an entanglement strand (Eqs. 35 and 16). This measures the conformational complexity at the length scale of entanglement strands. Our numerical results on linear FENE chains in a melt suggest that for long chains the entanglement strands may contain knots.

ACKNOWLEDGMENTS

This research was supported by a Swiss Government Scholarship with reference number 2011.0409.

Appendix A: Wormlike chains

Consider a *wormlike chain* (WLC), a connected linear string of $N-1$ segment unit vectors $\mathbf{u}_i = \mathbf{r}_{i+1} - \mathbf{r}_i$, that connect $N \gg 1$ nodes located at $\mathbf{r}_i$. With $\cos\,\theta_i = \mathbf{u}_i \cdot \mathbf{u}_{i+1}$ we may call $\theta_i \in [0, \pi]$ a *bending angle* between segments i and $i+1$. The hamiltonian of the discrete WLC is

$$H = -\kappa k_{\mathrm{B}} T \sum_{i=1}^{N-2} \cos\,\theta_i \tag{A1}$$

with dimensionless bending stiffness κ. Within the canonical ensemble the dimensionless *persistence length*, l_p, characterizing the orientational correlation of bonds,

$$\langle \mathbf{u}_i \cdot \mathbf{u}_j \rangle = \exp\left(-\frac{|i-j|}{l_p}\right), \tag{A2}$$

can be calculated analytically in terms of κ

$$l_p = -\frac{1}{\ln[\coth(\kappa) - 1/\kappa]}. \tag{A3}$$

At $\kappa \gg 1$ this rapidly approaches $l_p \approx \kappa - 1/2$, and $l_p = 1$ for $\kappa \approx 1.21$. The *Kuhn length* can be derived from the persistence length as $l_k \approx 2l_p$. The mean squared end-to-end distance of the WLC is analytically obtained from Eq. A2

$$\langle R^2 \rangle = 2 l_p L \left[1 - \frac{l_p}{L}\Big(1 - e^{-L/l_p}\Big)\right], \tag{A4}$$

where $L \equiv N-1$. The equilateral random walk exhibiting $\langle R^2 \rangle = L$ is recovered from Eq. A4 for $L \gg l_p = 1/2$ (or $\kappa \approx 0.4106$). The opposite extreme, a stiff chain exhibiting $\langle R^2 \rangle = L^2$ is recovered for $L \ll l_p \to \infty$ (i.e. large $\kappa \gg 1$).

WLCs with the correct statistics of the canonical ensemble can be grown segment-wise via Monte Carlo using random numbers x equally distributed over the interval $[0,1]$ as follows $\cos\theta_i = \kappa^{-1} \ln(2x \sinh\kappa)$. These bending angles give rise to the probability distribution $p(\theta) \sim \exp(\kappa\cos\theta)\sin\theta$. Employing $\int_0^\pi p(\theta) d\theta = 1$ one arrives at

$$p(\theta) = \frac{\kappa \exp(\kappa\cos\theta)\sin(\theta)}{2\sinh(\kappa)} \tag{A5}$$

Appendix B: The writhe of a chain with respect to its entanglement strands

Let us consider a polymer chain, I, with parametrization γ, formed by $Z+1$ entanglement strands, say $e_i, i = 1, \ldots, Z+1$, with parametrizations $\gamma_i, i = 1, \ldots, Z+1$ respectively. Then the writhe of I can be expressed as

$$\begin{aligned} Wr(I) &= \frac{1}{2\pi} \int_{[0,1]^*} \int_{[0,1]^*} \frac{(\dot\gamma(t), \dot\gamma(s), \gamma(t) - \gamma(s))}{|\gamma(t) - \gamma(s)|^3}\, \mathrm{d}t\mathrm{d}s \\ &= \frac{1}{2\pi} \sum_{i=1}^{Z+1} \int_{[0,1]^*} \int_{[0,1]^*} \frac{(\dot\gamma_i(t), \dot\gamma_i(s), \gamma_i(t) - \gamma_i(s))}{|\gamma_i(t) - \gamma_i(s)|^3}\, \mathrm{d}t\mathrm{d}s \\ &\quad + \frac{1}{2\pi} \sum_{i=1}^{Z} \sum_{j=i+1}^{Z+1} \int_{[0,1]} \int_{[0,1]} \frac{(\dot\gamma_i(t), \dot\gamma_j(s), \gamma_i(t) - \gamma_j(s))}{|\gamma_i(t) - \gamma_j(s)|^3}\, \mathrm{d}t\mathrm{d}s \\ &= \sum_{i=1}^{Z+1} Wr(e_i) + 2 \sum_{i=1}^{Z} \sum_{j=i+1}^{Z+1} L(e_i, e_j) \end{aligned} \tag{B1}$$

where $Wr(e_i)$ denotes the writhe of the entanglement strand e_i and $L(e_i, e_j)$ denotes the Gauss linking number of the entanglement strands i and j.

Appendix C: The mean squared writhe of an entanglement strand

The mean squared writhe of an entanglement strand in a chain averaged over all chains in a melt is given by Eq. 15, namely

$$\mathcal{W}_e^2 = \left\langle \frac{(Wr(I) - Wr(\mathrm{PP}(I)))^2}{Z+1} \right\rangle - 2\sum_{i<j} \left\langle \frac{Wr(e_i)Wr(e_j)}{Z+1} \right\rangle \tag{C1}$$

Consider the second term in the right side of C1. First recall that $Wr(e_i), Wr(e_j)$ are the writhe of the i-th and j-th entanglement strand of a chain respectively. As $N \to \infty$, N_e is expected to approach an asymptotic value [13]. Thus, for large enough N, Z and N_e are independent random variables. The writhe of an entanglement strand depends only on N_e, and thus for large N, it is also independent of Z. So, in the following we make the approximation

$$\left\langle \frac{Wr(e_i)Wr(e_j)}{Z+1} \right\rangle \approx \langle Wr(e_i)Wr(e_j)\rangle \left\langle \frac{1}{Z+1} \right\rangle \tag{C2}$$

Next we notice that each entanglement strand is a random polymer chain, independent of the other entanglement strands, so the terms $Wr(e_i)$ and $Wr(e_j)$ are independent random variables, and thus, $\langle Wr(e_i)Wr(e_j)\rangle = \langle Wr(e_i)\rangle\langle Wr(e_j)\rangle$. But $\langle Wr(e_i)\rangle$ is independent of the index i, thus $\langle Wr(e_i)\rangle = \langle Wr(e_j)\rangle = \langle Wr(e)\rangle$. Since each entanglement strand in the space of configurations can have positive or negative writhe with the same probability, $\langle Wr(e_i)\rangle = \langle Wr(e_j)\rangle = \langle Wr(e)\rangle = 0$. Thus, the second term in the right side of C1 vanishes, and Eq. C1 becomes

$$\mathcal{W}_e^2 \approx \left\langle \frac{[Wr(I) - Wr(\mathrm{PP}(I))]^2}{Z+1} \right\rangle. \tag{C3}$$

Appendix D: Distribution of $\mathcal{N}_e$

In [15], the probability distribution of the number of kinks, Z, per chain is given by a Poissonean

$$p(Z) = \frac{\mu^{Z-1}e^{-\mu}}{(Z-1)!}, \qquad \sum_{Z=0}^{\infty} p(Z) = 1 \tag{D1}$$

where $1 + \mu = \mathcal{Z} = \sum_{Z=0}^{\infty} Zp(Z)$. The probability distribution of $\mathcal{N}_e = N/Z$ values for single chains, $P(\mathcal{N}_e)$, is obtained from $p(Z)$ via $P(\mathcal{N}_e)d\mathcal{N}_e = p(Z)dZ$, more precisely,

$$\begin{aligned} P(\mathcal{N}_e) &= \left|\frac{dZ}{d\mathcal{N}_e}\right| p(Z) = \frac{N}{\mathcal{N}_e^2} p\left(\frac{N}{\mathcal{N}_e}\right) \\ &= \frac{N\mu^{N/\mathcal{N}_e - 1}e^{-\mu}}{\mathcal{N}_e^2 \Gamma(N/\mathcal{N}_e)}. \end{aligned} \tag{D2}$$

where Γ is the Gamma function.

[1] M. Doi and S. F. Edwards, *The Theory of Polymer Dynamics* (Clarendon Press, Oxford, 1986).
[2] L. J. Fetters, D. J. Lohse, D. Richter, T. A. Witten, and A. Zirkel, Macromolecules **27**, 4639 (1994).
[3] L. J. Fetters, D. J. Lohse, S. T. Milner, and W. W. Graessly, Macromolecules **32**, 6847 (1999).
[4] M. Kröger and S. Hess, Phys. Rev. Lett. **85**, 1128 (2000).
[5] M. Rubinstein and E. J. Helfand, J. Chem. Phys. **82**, 2477 (1984).
[6] R. Everaers, S. K. Sukumaran, G. S. Grest, C. Svaneborg, A. Sivasubramanian, and K. Kremer, Science **303**, 823 (2004).
[7] M. Kröger, Comput. Phys. Commun. **168**, 209 (2005).
[8] S. Shanbhag and M. Kröger, Macromolecules **40**, 2897 (2007).
[9] C. Tzoumanekas and D. N. Theodorou, Macromolecules **39**, 4592 (2006).
[10] M. Kröger, J. Ramirez, and H. C. Öttinger, Polymer **43**, 477 (2002).
[11] Z1 is available online at http://www.complexfluids.ethz.ch/Z1.
[12] M. Pütz and K. Kremer, Europhys. Lett. **49**, 735 (2000).
[13] R. S. Hoy, K. Foteinopoulou, and M. Kröger, Phys. Rev. E **80**, 031803 (2009).
[14] S. K. Sukumaran, G. S. Grest, K. Kremer, and R. Everaers, R. J. Polym. Sci. B Polym. Phys. **43**, 917 (2005).
[15] K. Foteinopoulou, N. C. Karayiannis, V. G. Mavrantzas, and M. Kröger, Macromolecules **39**, 4207 (2006).
[16] S. Shanbhag and R. G. Larson, Phys. Rev. Lett. **94**, 076001 (2005).
[17] S. Shanbhag and R. G. Larson, Macromolecules **39**, 2413 (2006).
[18] Q. Zhou and R. G. Larson, Macromolecules **38**, 5761 (2005).
[19] K. Kremer and G. S. Grest, J. Chem. Phys. **92**, 5057 (1990).
[20] D. J. Read, K. Jagannathan, and A. E. Likhtman, Macromolecules **41**, 6843 (2008).
[21] W. Bisbee, J. Qin, and S. T. Milner, Macromolecules **44**, 8972 (2011).
[22] F. Edwards, Proc Phys Soc **91**, 513 (1967).
[23] F. Edwards, J Phys A: Gen Phys **1**, 15 (1968).
[24] P. Freyd, D. Yetter, J. Hoste, W. Lickorish, K. Millett, and A. Ocneanu, Bull. Am. Math. Soc. **12**, 239 (1985).
[25] J. Przytycki and P. Traczyk, Proc. Amer. Math. Soc. **100**, 744 (1987).
[26] V. Jones, Bull. Am. Math. Soc. **12**, 103 (1985).
[27] L. H. Kauffmann, *Knots and Physics*, Series on knots and everything, Vol. 1 (World Scientific, 1991).
[28] K. Iwata and S. F. Edwards, J Chem Phys **90**, 084567 (1989).
[29] K. Foteinopoulou, N. C. Karayiannis, M. Laso, M. Kröger, and L. Mansfield, Phys. Rev. Lett. **101**, 265702 (2008).
[30] J. Qin and S. T. Milner, Soft Matter **7**, 10676 (2011).
[31] C. Micheletti, D. Marenduzzo, and E. Orlandini, Phys. Rep. **504**, 1 (2011).

[32] A. Stasiak, V. Katritch, and L. Kauffman, *Ideal knots*, Series on knots and everything, Vol. 19 (World Scientific, 1999).

[33] E. Flapan, *When topology meets chemistry: a topological look at molecular chirality* (Cambridge University Press, 2000).

[34] M. Laso, N. C. Karayiannis, K. Foteinopoulou, L. Mansfield, and M. Kröger, Soft Matter **5**, 1762 (2009).

[35] K. Millett, A. Dobay, and A. Stasiak, Phys. Rev. Lett. **38**, 601 (2004).

[36] J. I. Sulkowska, E. J. Rawdon, K. C. Millett, J. N. Onuchic, and A. Stasiak, PNAS **109**, E1715 (2012).

[37] P. K. Agarwal, H. Edelsbrunner, and W. Y., Discrete Comput. Geom. **32**, 37 (2004).

[38] Y. Diao, A. Dobay, and A. Stasiak, J. Phys. A: Math. Gen. **38**, 7601 (2005).

[39] K. Klenin and J. Langowski, Biopolymers **54**, 307 (2000).

[40] M. A. Berger and C. Prior, J. Phys. A. **39**, 8321 (2006).

[41] C. Laing and D. W. Sumners, J. Phys. A **39**, 3535 (2006).

[42] C. Laing and D. W. Sumners, J. Knot Theor. Ramif. **12**, 41 (2007).

[43] W. R. Bauer, F. H. C. Crick, and J. H. White, Sci. Am. **243**, 118 (1980).

[44] T. Blackstone, P. McGuirck, C. Laing, M. Vazquez, J. Roca, and J. Arsuaga, Proc. Int. Workshop Knot Theory for Scientific Objects OCAMI Studies **1**, 239 (2007).

[45] P. Hoidn, R. B. Kusner, and A. Stasiak, New J. Phys. **4**, 1 (2002).

[46] C. Micheletti, D. Marenduzzo, E. Orlandini, and D. W. Sumners, J. Chem. Phys. **124**, 64903.1 (2006).

[47] H. K. Moffatt, J. Fluid Mech. **35**, 117 (1969).

[48] H. K. Moffatt and R. L. Ricca, Proc. R. Soc. London Sec. A **439**, 411 (1992).

[49] E. Orlandini and W. S. G., J. Chem. Phys. **121**, 12094 (2004).

[50] E. Orlandini and S. G. Whittington, Rev. Mod. Phys. **79**, 611 (2007).

[51] E. Orlandini, M. C. Tesi, and S. G. Whittington, J. Phys. A: Math. Gen. **33**, L181 (2000).

[52] J. Arsuaga, T. Blackstone, Y. Diao, K. Hinson, E. Karadayi, and M. Saito, J. Phys. A: Math. Theor. **40**, 11697 (2007).

[53] Y. Diao, N. Pippenger, and D. W. Sumners, J. Knot Theor. Ramif. **3**, 419 (1993).

[54] Y. Diao, J. Knot Theor. Ramif. **4**, 189 (1995).

[55] N. Pippenger, Discrete Appl. Math. **25**, 273 (1989).

[56] D. W. Sumners and S. G. Whittington, J. Phys. A: Math. Gen. **21**, 1689 (1988).

[57] S. G. Whittington, Proc. Symp. Appl. Math. **45**, 73 (1992).

[58] J. Arsuaga, Y. Diao, and M. Vazquez, in Mathematics of DNA Structure, Functions and Interactions, edited C. J. Benham, S. Harvey, W. K. Olson, D. W. Sumners and D. Swigon (New York: Springer Science + Business Media) **40**, 7 (2009).

[59] M. Tesi, E. Janse van Rensbourg, E. Orlandini, and S. G. Whittington, J. Phys. A: Math. Gen. **27**, 347 (1994).

[60] E. Orlandini, M. C. Tesi, S. G. Whittington, D. W. Sumners, and E. J. J. van Rensburg, J. Phys. A: Math. Gen. **27**, L333 (1994).

[61] E. J. J. van Rensburg, E. Orlandini, D. W. Sumners, M. C. Tesi, and S. G. Whittington, J. Phys. A: Math. Gen. **26**, L981 (1993).

[62] E. Panagiotou, K. C. Millett, and S. Lambropoulou, J. Phys. A: Math. Theor. **43**, 045208 (2010).

[63] J. Portillo, Y. Diao, R. Scharein, J. Arsuaga, and M. Vazquez, J. Phys. A: Math. Theor. **44**, 275004 (2011).

[64] A. L. Kholodenko and T. A. Vilgis, J. Phys. A: Math. Gen. **29**, 939 (1996).

[65] S. Anogiannakis, C. Tzoumanekas, and D. N. Theodorou, Macromolecules **45**, 9475 (2012).

[66] K. Foteinopoulou, N. C. Karayiannis, M. Laso, and M. Kröger, J. Phys. Chem. B **113**, 442 (2009).

[67] K. F. Gauss, Kgl. Gesellsch. Wiss. Göttingen **5**, 605 (1877).

[68] E. Panagiotou, C. Tzoumanekas, S. Lambropoulou, K. C. Millett, and D. N. Theodorou, Progr. Theor. Phys. Suppl. **191**, 172 (2011).

[69] E. Panagiotou, K. C. Millett, and S. Lambropoulou, in Procedia IUTAM: Topological Fluid Dynamics, Edited by H.K. Moffatt, K. Bajer and Y. Kimura (Elsevier) **7**, 251 (2013).

[70] Y. Diao, R. N. Kushner, K. Millett, and A. Stasiak, J. Phys. A: Math. Gen. **36**, 11561 (2003).

[71] J. Arsuaga, T. Blackstone, Y. Diao, E. Karadayi, and M. Saito, J. Phys. A: Math. Theor. **40**, 1925 (2007).

[72] M. Rubinstein and R. Colby, *Polymer Physics* (Oxford University Press, 2003).

[73] E. J. Rawdon, J. C. Kern, M. Piatek, P. Plunkett, A. Stasiak, and K. C. Millett, Macromolecules **41**, 8281 (2008).

[74] T. C. B. McLeish, Adv. Phys. **51**, 1379 (2002).

[75] P. G. de Gennes, *Scaling concepts in Polymer Physics* (Cornell University Press, 1979).

[76] C. Baig, V. G. Mavrantzas, and M. Kröger, Macromolecules **43**, 6996 (2010).

[77] M. Kröger, Phys. Rep. **390**, 453 (2004).

[78] M. Kröger, Comput. Phys. Commun. **118**, 278 (1999).

[79] R. Everaers and K. Kremer, Phys. Rev. E. **14**, 55 (1996).

[80] C. Tzoumanekas, F. Lahmar, B. Rousseau, and D. N. Theodorou, Macromolecules **42**, 7474 (2009).

[81] F. Lahmar, C. Tzoumanekas, D. N. Theodorou, and B. Rousseau, Macromolecules **42**, 7485 (2009).